

Automating scattering amplitudes with chirality flow

Andrew Lifson¹, Malin Sjödal¹ and Zenny Wettersten¹

Department of Astronomy and Theoretical Physics, Lund University, Box 43, 221 00 Lund, Sweden

March 28, 2022

Abstract. Recently we introduced the chirality-flow formalism, a method which builds on the spinor-helicity formalism and is inspired by the color-flow idea in QCD. With this formalism, Feynman rules and diagrams are simplified to the extent that it is often possible to immediately, by hand, write down a helicity amplitude given a Feynman diagram. In this paper we show that the method can also speed up numerical evaluation of scattering amplitudes by considering e^+e^- going to n photons in a MADGRAPH-based tree-level implementation. We find that the computation time is reduced by roughly a factor ten for six photons, and that it scales better with the number of external particles than the default MADGRAPH5_AMC@NLO implementation. This performance gain is in part attributed to the more compact Lorentz structures involved, and in part due to a transparent choice of gauge reference vectors which reduces the number of Feynman diagrams considered.

1 Introduction

Event generators [1–5] for scattering amplitudes are indispensable tools for calculating cross sections and understanding event topologies at collider experiments.

At the core of amplitude calculations is the evaluation of the hard scattering matrix element, typically calculated using Feynman diagram techniques as helicity amplitudes [1, 2, 6], i.e., amplitudes with assigned helicities.

While such calculations may well be performed using the full four-dimensional Dirac spinors, simplifications can be achieved using the spinor-helicity [7–22] and Weyl-van der Waerden [1, 23–31] formalisms, in which spinors are decomposed into their **left**- and **right**-chiral parts which transform separately as different $SL(2, \mathbb{C})$ copies (see e.g. [32–36] for pedagogical introductions). The Dirac spinors are thus split into

$$u(p) \sim v(p) \sim \begin{pmatrix} [p_1] \\ p_2 \rangle \end{pmatrix}, \quad \bar{u}(p) \sim \bar{v}(p) \sim ([p_1|, \langle p_2|),$$

for some p_1 and p_2 , one of which reduces to p in the ultrarelativistic/massless case, while the other vanishes.¹

Here the **square** brackets are Weyl spinors transforming under $SL(2, \mathbb{C})_L$ and the **angled** brackets are Weyl spinors transforming under $SL(2, \mathbb{C})_R$.

Since the only invariant tensor for $SL(2, \mathbb{C})$ is the fully antisymmetric Levi-Civita tensor, $\epsilon^{12} = -\epsilon^{21} = \epsilon_{21} =$

$-\epsilon_{12} = 1$, invariant spinor inner products are formed by contractions with this tensor

$$\underbrace{\epsilon^{\alpha\beta} [i]_\beta [j]_\alpha}_{\equiv \langle i|^\alpha} = \langle i|^\alpha [j]_\alpha = \langle ij \rangle = -\langle ji \rangle,$$

$$\underbrace{\epsilon_{\dot{\alpha}\dot{\beta}} [i]^{\dot{\beta}} [j]^{\dot{\alpha}}}_{\equiv [i]_{\dot{\alpha}}} = [i]_{\dot{\alpha}} [j]^{\dot{\alpha}} = [ij] = -[ji],$$

where we denote $\langle p_i| = \langle i|$ etc., for brevity, and where (up to a phase) $\langle ij \rangle \sim [ij] \sim \sqrt{2p_i \cdot p_j}$.

Since these are the only invariant structures at hand, it can be anticipated that all scattering amplitudes should be expressible in terms of these spinor inner products, and that depicting the contraction with a connecting line, one can obtain a “flow” picture for the Lorentz structure.

This flow picture, the chirality-flow formalism is introduced in the next section, along with an illuminating example of how to write down amplitudes. In the subsequent section, section 3, we describe our chirality-flow implementation based on the MADGRAPH5_AMC@NLO framework [2]. After that, the obtained speed gain is digested in section 4. Finally, concluding remarks and an outlook are given in section 5.

2 Chirality flow

In the chirality-flow formalism [37–40] we take the simplifications of the spinor-helicity formalism one step further. By proving that we can recast Feynman rules to be represented in terms of flows between external spinors, we manage to simplify Feynman rules and diagrams to the

¹ While this paper deals with massless particles, massive fermions can easily be treated. For example, an outgoing spinor of positive helicity and mass m is $\bar{u}^+(p) = \left([p_f|, \frac{m}{\langle p_b p_f \rangle} \langle p_b| \right)$, where p_f and p_b are the forward and backward components of the momentum p , i.e., $p_{f/b} = \frac{p^0 \pm |\vec{p}|}{2} (1, \pm \hat{p})$ [16, 30, 31, 37].

extent that helicity amplitudes can often be immediately written down given a Feynman diagram.

Introducing graphical flow representations [39] for the external spinors,

$$\begin{aligned} \langle i | &= \text{circle} \leftarrow i & , & \quad | i \rangle = \text{circle} \leftarrow i & , \\ | j \rangle &= \text{circle} \rightarrow j & , & \quad | j \rangle = \text{circle} \rightarrow j & , \end{aligned}$$

we can — in analogy with the color-flow representation of gluons in QCD — obtain a double line representation for external spin-1 particles. Letting $\epsilon_L(p_i, r)$ denote a left-chiral (negative helicity incoming or positive helicity outgoing) photon of momentum p_i and with gauge reference vector r , and similarly $\epsilon_R(p_i, r)$ denote a right-chiral (positive helicity incoming or negative helicity outgoing) photon, we have

$$\begin{aligned} \epsilon_L(p_i, r) &\rightarrow \frac{1}{\langle ri \rangle} \text{circle} \leftarrow r \rightarrow i & \text{or} & \quad \frac{1}{\langle ri \rangle} \text{circle} \rightarrow r \leftarrow i & , \\ \epsilon_R(p_i, r) &\rightarrow \frac{1}{[ir]} \text{circle} \leftarrow r \rightarrow i & \text{or} & \quad \frac{1}{[ir]} \text{circle} \rightarrow r \leftarrow i & . \end{aligned}$$

Note that the unphysical reference momentum r is carried by the right-chiral line for a left-chiral photon, and vice versa.

In [39], we proved that we can always use the Fierz identity

$$\langle i | \bar{\tau}^\mu | j \rangle [k | \tau_\mu | l \rangle = \langle il | [kj \rangle$$

on Dirac matrices decomposed into the Pauli matrices², $\tau^\mu = \sigma^\mu / \sqrt{2}$, combined with charge conjugation (see e.g. [33, 35])

$$\langle i | \bar{\tau}^\mu | j \rangle = [j | \tau^\mu | i \rangle$$

to replace a photon (spin-1) propagator by a solid and a dotted line with arrows opposing

$$\begin{aligned} -i \frac{g_{\mu\nu}}{p^2} &= \mu \text{ wavy line } \nu \xrightarrow{p} \rightarrow \\ -\frac{i}{p^2} \text{ solid } \leftarrow \text{dotted} &\text{ or } -\frac{i}{p^2} \text{ dotted } \leftarrow \text{solid} . \end{aligned}$$

The arrow direction, for internal as well as external photons, has to be chosen such that the arrows in the diagram align with each other (rather than oppose each other).

This also enables us to recast the fermion-photon (spin-1) vertex into a simple flow form

$$\begin{aligned} ie\sigma^\mu &= \begin{array}{c} L \\ \nearrow \\ \text{wavy } \mu \\ \nwarrow \\ R \end{array} \rightarrow ie\sqrt{2} \begin{array}{c} \text{dotted } \leftarrow \\ \text{solid } \rightarrow \end{array} , \\ ie\bar{\sigma}^\mu &= \begin{array}{c} R \\ \nearrow \\ \text{wavy } \mu \\ \nwarrow \\ L \end{array} \rightarrow ie\sqrt{2} \begin{array}{c} \text{solid } \leftarrow \\ \text{dotted } \rightarrow \end{array} . \end{aligned}$$

² This normalization of the Pauli matrices is chosen to avoid carrying and canceling unnecessary factors of $\sqrt{2}$.

The fermion propagator requires some more consideration, but the parts contracted with σ and $\bar{\sigma}$ can be represented graphically by

$$\begin{aligned} \frac{i}{p^2} p_\mu \sigma^\mu &= \frac{i}{p^2} \not{p} \rightarrow \frac{i}{p^2} \text{dotted } \rightarrow \text{solid} \xrightarrow{p} \text{circle} \rightarrow \text{solid} & \text{and} \\ \frac{i}{p^2} p_\mu \bar{\sigma}^\mu &= \frac{i}{p^2} \bar{\not{p}} \rightarrow \frac{i}{p^2} \text{solid } \rightarrow \text{circle} \rightarrow \text{dotted} , \end{aligned}$$

respectively.

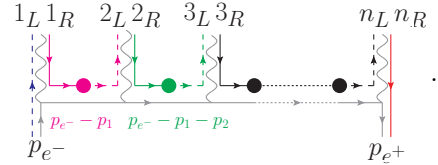
Decomposed into massless momenta p_i , with $p = \sum_i p_i$, $p_i^2 = 0$, we have for the first term

$$\text{dotted } \rightarrow \text{solid} \xrightarrow{p} \text{circle} \rightarrow \text{solid} = \sum_i \text{dotted } \rightarrow \text{circle} \rightarrow \text{solid} \xrightarrow{p_i} \text{circle} \rightarrow \text{solid} ,$$

and similar for the second term.

Applying these rules, it is possible to directly write down scattering amplitudes, either in terms of slashed momenta or in terms of Lorentz-invariant spinor inner products.

Calculations with Feynman diagrams can then be simplified in an unprecedented manner, making them trivial. To illustrate this, we consider a Feynman diagram relevant for $e_R^+ e_L^- \rightarrow n$ photons, and overlay the chirality-flow representation



Here, for a left-chiral photon $1_L = p_1$ and $1_R = r_1$, and vice versa for a right-chiral photon, and we have used the freedom to assign chirality-flow arrows in any consistent direction.

Writing down the amplitude (as an example for photon 1 right-chiral, and photons 2 and 3 left-chiral), either in terms of $\sigma/\bar{\sigma}$ matrices,

$$\begin{aligned} &\underbrace{(\sqrt{2}ie)^n}_{\text{from vertices}} \underbrace{\frac{(i)^{n-1}}{(p_{e^-} - p_1)^2 \dots}}_{\text{from fermion propagators}} \underbrace{\frac{1}{[1_L 1_L] \langle 2_R 2 \rangle \langle 3_R 3 \rangle \dots}}_{\text{from polarization vectors}} \\ &\times [p_{e^-} 1_L] \times \langle 1_R | \bar{\not{p}}_{e^- - 1} | 2_L \rangle \times \langle 2_R | \bar{\not{p}}_{e^- - 1 - 2} | 3_L \rangle \\ &\times \dots \times \langle n_R p_{e^+} \rangle , \end{aligned} \quad (1)$$

or with the spinor structure directly expressed in terms of spinor inner products,

$$\begin{aligned} &[p_{e^-} 1_L] \times \left(\langle 1_R p_{e^-} \rangle [p_{e^-} 2_L] - \langle 1_R 1 \rangle [1 2_L] \right) \\ &\times \left(\langle 2_R p_{e^-} \rangle [p_{e^-} 3_L] - \langle 2_R 1 \rangle [1 3_L] - \langle 2_R 2 \rangle [2 3_L] \right) \\ &\times \dots \times \langle n_R p_{e^+} \rangle , \end{aligned} \quad (2)$$

we see that this diagram vanishes if the reference momentum $r_1 = 1_L$ is chosen to be p_{e^-} , since $[p_{e^-} p_{e^-}] = 0$,

i.e. for a right-chiral photon, this diagram can be chosen to disappear. By picking the gauge vector to be p_{e^-} for all right-chiral photons, we can make all diagrams with a right-chiral photon attached directly to the electron disappear. Similarly, by letting the reference momentum be p_{e^+} for all left-chiral photons, diagrams with a left-chiral photon attached next to p_{e^+} vanish.

If a given assignment of photon chiralities has n_L left-chiral photons and n_R right-chiral photons, then we have n_L non-vanishing ways of placing a photon next to the electron, n_R ways to place a photon next to the positron, and $(n-2)!$ possible ways to order the remaining photons. This leaves us with $n_L n_R (n-2)!$, rather than $n!$ diagrams to consider for this chirality assignment, a simplification which turns out to reduce the computation time significantly.

By consistently using this gauge choice, diagram generation can be constructed to recognize any vertices coupling a left-chiral (right-chiral) photon with the right-chiral (left-chiral) fermion as not contributing to the amplitude, and the diagrams can be removed already before compile time. We refer to this process as *gauge based diagram removal*.

We note that the same simplification could have been achieved within the spinor-helicity or Weyl-van der Waerden formalisms, but with chirality flow it is completely transparent.

3 MadGraph implementation

To test the viability of a numerical implementation of chirality flow, we create a UFO [41] model with chiral particles and vertices, feed this into the software framework `MADGRAPH5_AMC@NLO(MG5aMC)` [2] in standalone mode, and repurpose the amplitude evaluations to work within the chirality-flow formalism.

To make the current helicity amplitude evaluation and our implementation as comparable as possible, we follow the structure of MG5aMC wherever possible. We therefore only 1) modify MG5aMC's diagram generation in order to produce chirality-flow diagrams, and 2) replace the underlying numerical HELAS-like routines generated by ALOHA [42] for calculating off-shell currents and amplitudes with a similar library performing these calculations based on chirality flow.

Although this implementation does not lend itself immediately to all the possible benefits of the chirality-flow formalism, it does make runtime comparisons as fair as possible³, as we are performing the same type of evaluations of the same type of processes using the same type of program. Any advantage in evaluation time will thus be due to simplified calculations (involving smaller Lorentz

structures) or a reduced *number* of evaluations (as for gauge based diagram removal).

The evaluation process performed in our implementation is identical to the MG5aMC version, although with explicitly chiral particles and vertices. As MG5aMC treats different helicity states of a particle as the same type of particle, this means that our implementation runs what in MG5aMC is a helicity state as its own process. If we wish to perform a helicity summed calculation, as in standalone MG5aMC, we need to run each chirality configuration as its own subprocess. This brings about some overhead⁴.

Aside from generating chirality-flow diagrams, rather than standard Feynman diagrams, we also replace the libraries for the matrix element evaluations with a library performing the corresponding calculations using chirality flow. However, as MG5aMC stores particle momenta locally at each vertex evaluation, the decomposition of the fermion propagator momentum is based on eq. (1) rather than eq. (2). Changing this and implementing caching of spinor inner products could likely offer additional speed gain.

To validate our implementation, several classes of processes were evaluated at random points in phase space and compared with the same processes evaluated at the same phase space points using default MG5aMC. The processes validated include $e^+e^- \rightarrow n\gamma$, $2 \leq n \leq 4$; $e^+e^- \rightarrow \mu^+\mu^-n\gamma$, $0 \leq n \leq 2$; $e^+e^- \rightarrow e^+e^-n\gamma$, $0 \leq n \leq 2$; $e^-\gamma \rightarrow e^-n\gamma$, $1 \leq n \leq 3$; $e^+e^- \rightarrow 2\mu^+2\mu^-$; $e^+e^- \rightarrow e^+e^-\mu^+\mu^-$; and $e^-\mu^- \rightarrow 2e^-\mu^-e^+$, for all possible helicity configurations. All amplitudes were found to be equal within numerical precision.

4 Results

Figure 1 depicts measured runtimes for evaluation of 100 000 matrix elements for the process $e^+e^- \rightarrow n\gamma$ as a function of photon multiplicity n (measured on an AMD Ryzen 5 1600 CPU). Three implementations are depicted: MG5aMC (solid blue line), our implementation without gauge based diagram removal (dotted orange line), and our implementation with gauge based diagram removal (dashed red line). These matrix elements were evaluated for phase space points generated by RAMBO [44], all using the same seed. The comparison of the dotted and solid lines shows the improved evaluation speed obtained by performing calculations using the simplified Lorentz structure, whereas the difference between the dotted line and the dashed line is due to gauge based diagram removal.

For this comparison, MG5aMC has been manually set to consider only contributing helicity configurations, and

³ Since we use standalone output, some optimizations such as the recently implemented helicity recycling [43] are not included in the MG5aMC speed (though this recycling will in theory equally apply to chirality flow). Rather, the comparison we make singles out the gains due to simpler Lorentz structures and gauge based diagram removal.

⁴ As each helicity configuration is computed as a distinct process, phase space points are generated independently for each process using the RAMBO algorithm [44]. For the simplest process $e^+e^- \rightarrow 2\gamma$, an analysis with Valgrind [45, 46] shows that RAMBO ends up taking roughly half of the runtime for our implementation, whereas the time used by RAMBO is negligible for many photons.

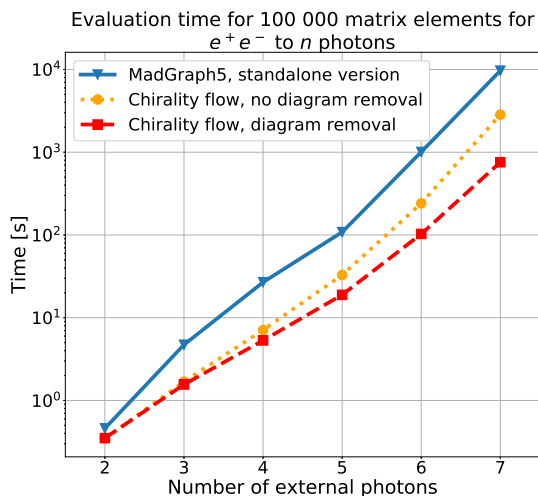


Fig. 1: Measured runtimes for evaluation of 100 000 matrix elements for MG5aMC and our implementation, as a function of photon multiplicity n . The dotted orange curve depicts the chirality-flow implementation without gauge based diagram removal, whereas the dashed red curve includes gauge based diagram removal. The same number of helicity/chirality configurations are evaluated in all cases. The chirality-flow implementations evaluate matrix elements faster than MG5aMC for all n . For small n the gain can be explained almost fully by simplified calculations, but for larger n the effects of gauge based diagram removal become readily apparent.

subprocesses where all external photons have the same chirality have been discarded for the implementation without diagram removal⁵. With this setup, all three program versions will evaluate the same number of matrix elements for the same number of helicity/chirality configurations.

As can be seen in Figure 1, the chirality-flow implementations perform the evaluations faster than MADGRAPH5 for all photon multiplicities n . Additionally, for small n both chirality-flow versions scale better with n than MG5aMC, and chirality flow with gauge based diagram removal maintains this gentler slope with n into the region of large n .

In the small n region, $n \lesssim 4$, the difference between MG5aMC and chirality flow is explained almost entirely by the simplified Lorentz structures, but as the large n region is approached, $n \gtrsim 5$, the benefit of gauge based diagram removal becomes clear. At $n = 6$, chirality flow with diagram removal is roughly a factor 10 faster than MG5aMC.

⁵ MG5aMC standalone has a routine for detecting non-contributing helicity configurations. For the process we consider, this routine discards configurations where the fermions have the same helicity, but it does not discard configurations where all photons have the same helicity (using MADGRAPH5_AMC@NLO 3.2.0, with standalone output, released on August 22nd, 2021).

5 Conclusion and outlook

In previous articles, we have developed chirality flow and shown its benefits for analytic calculations. Here, we have further demonstrated the viability of the chirality-flow formalism in a numerical MG5aMC implementation.

As Figure 1 demonstrates, our chirality-flow based implementation evaluates matrix elements faster than standalone MG5aMC. This speed increase is due to two different factors. The first is the simplified calculations obtained by performing evaluations of Lorentz structures in the chirality-flow formalism. The second, however, is an additional benefit of chirality flow: the effect of gauge reference vector choice becomes very transparent. Since the effects of a given reference momentum can be seen directly from the chirality-flow diagrams, a good choice is immediately discernible. Combining these two effects, the process $e^+e^- \rightarrow n\gamma$ ends up being evaluated roughly ten times faster for $n \geq 6$ in our implementation, with speed gain increasing for an increasing number of photons.

In this paper, the MG5aMC structure has been maintained for the purpose of comparison. However, the HELAS-based structure used by MG5aMC is not naturally suited for chirality flow, since it evaluates diagrams by calculating off-shell particle wavefunctions at vertices, before combining them to calculate an amplitude. This general structure allows recycling of currents for each diagram where the given current enters.

For chirality flow, another natural object to recycle is the spinor inner products (cf. eq. (2)). Since the amplitude corresponding to a given chirality-flow diagram can be expressed by a small number of these scalars, caching them is likely to increase the evaluation speed even further in future implementations.

While this implementation has concerned only massless QED, the chirality-flow formalism has been developed for the full massive Standard Model [37], and sizable speed gains could likely be attained for a large class of phenomenologically relevant Standard Model processes.

Acknowledgments

We thank Olivier Mattelaer for useful discussions on the MG5aMC implementation. This work was supported by the Swedish Research Council (contract number 2016-05996, as well as the European Union’s Horizon 2020 research and innovation programme (grant agreement No 668679). This work has also been supported in part by the European Union’s Horizon 2020 research and innovation programme as part of the Marie Skłodowska-Curie Innovative Training Network MCnetITN3 (grant agreement no. 722104).

References

1. T. Gleisberg and S. Hoeche, *Comix, a new matrix element generator*, *JHEP* **12** (2008) 039 [0808.3674].

2. J. Alwall, R. Frederix, S. Frixione, V. Hirschi, F. Maltoni, O. Mattelaer et al., *The automated computation of tree-level and next-to-leading order differential cross sections, and their matching to parton shower simulations*, *JHEP* **07** (2014) 079 [1405.0301].
3. T. Sjöstrand, S. Ask, J. R. Christiansen, R. Corke, N. Desai, P. Ilten et al., *An introduction to PYTHIA 8.2*, *Comput. Phys. Commun.* **191** (2015) 159 [1410.3012].
4. J. Bellm et al., *Herwig 7.0/Herwig++ 3.0 release note*, *Eur. Phys. J. C* **76** (2016) 196 [1512.01178].
5. SHERPA collaboration, E. Bothmann et al., *Event Generation with Sherpa 2.2*, *SciPost Phys.* **7** (2019) 034 [1905.09127].
6. H. Murayama, I. Watanabe and K. Hagiwara, *HELAS: HELicity amplitude subroutines for Feynman diagram evaluations*, tech. rep., 1, 1992.
7. P. De Causmaecker, R. Gastmans, W. Troost and T. T. Wu, *Multiple Bremsstrahlung in Gauge Theories at High-Energies. 1. General Formalism for Quantum Electrodynamics*, *Nucl. Phys.* **B206** (1982) 53.
8. F. A. Berends, R. Kleiss, P. De Causmaecker, R. Gastmans and T. T. Wu, *Single Bremsstrahlung Processes in Gauge Theories*, *Phys. Lett.* **103B** (1981) 124.
9. F. A. Berends, R. Kleiss, P. De Causmaecker, R. Gastmans, W. Troost and T. T. Wu, *Multiple Bremsstrahlung in Gauge Theories at High-Energies. 2. Single Bremsstrahlung*, *Nucl. Phys.* **B206** (1982) 61.
10. P. De Causmaecker, R. Gastmans, W. Troost and T. T. Wu, *Helicity Amplitudes for Massless QED*, *Phys. Lett.* **105B** (1981) 215.
11. CALKUL collaboration, F. A. Berends, R. Kleiss, P. de Causmaecker, R. Gastmans, W. Troost and T. T. Wu, *Multiple Bremsstrahlung in Gauge Theories at High-energies. 3. Finite Mass Effects in Collinear Photon Bremsstrahlung*, *Nucl. Phys.* **B239** (1984) 382.
12. R. Kleiss, *The Cross-section for $e^+e^- \rightarrow e^+e^-e^+e^-$* , *Nucl. Phys.* **B241** (1984) 61.
13. F. A. Berends, P. H. Daverveldt and R. Kleiss, *Complete Lowest Order Calculations for Four Lepton Final States in electron-Positron Collisions*, *Nucl. Phys.* **B253** (1985) 441.
14. J. F. Gunion and Z. Kunszt, *Four jet processes: gluon-gluon scattering to nonidentical quark - anti-quark pairs*, *Phys. Lett.* **159B** (1985) 167.
15. J. F. Gunion and Z. Kunszt, *Improved Analytic Techniques for Tree Graph Calculations and the $G g q$ anti- q Lepton anti-Lepton Subprocess*, *Phys. Lett.* **161B** (1985) 333.
16. R. Kleiss and W. J. Stirling, *Spinor Techniques for Calculating p anti- $p \rightarrow W^\pm / Z^0 +$ Jets*, *Nucl. Phys.* **B262** (1985) 235.
17. K. Hagiwara and D. Zeppenfeld, *Helicity Amplitudes for Heavy Lepton Production in e^+e^- Annihilation*, *Nucl. Phys.* **B274** (1986) 1.
18. R. Kleiss, *Hard Bremsstrahlung Amplitudes for e^+e^- Collisions With Polarized Beams at LEP / SLC Energies*, *Z. Phys.* **C33** (1987) 433.
19. R. Kleiss and W. J. Stirling, *Cross-sections for the Production of an Arbitrary Number of Photons in Electron - Positron Annihilation*, *Phys. Lett.* **B179** (1986) 159.
20. Z. Xu, D.-H. Zhang and L. Chang, *Helicity Amplitudes for Multiple Bremsstrahlung in Massless Nonabelian Gauge Theories*, *Nucl. Phys.* **B291** (1987) 392.
21. CALKUL collaboration, R. Gastmans, F. A. Berends, D. Danckaert, P. De Causmaecker, R. Kleiss, W. Troost et al., *New techniques and results in gauge theory calculations*, in *Electroweak effects at high-energies. Proceedings, 1st Europhysics study conference, Erice, Italy, February 1-12, 1983*, pp. 599–609, 1987.
22. C. Schwinn and S. Weinzierl, *Scalar diagrammatic rules for Born amplitudes in QCD*, *JHEP* **05** (2005) 006 [hep-th/0503015].
23. G. R. Farrar and F. Neri, *How to Calculate 35640 $O(\alpha^5)$ Feynman Diagrams in Less Than an Hour*, *Phys. Lett.* **130B** (1983) 109.
24. F. A. Berends and W. Giele, *The Six Gluon Process as an Example of Weyl-Van Der Waerden Spinor Calculus*, *Nucl. Phys.* **B294** (1987) 700.
25. F. A. Berends and W. T. Giele, *Recursive Calculations for Processes with n Gluons*, *Nucl. Phys.* **B306** (1988) 759.
26. F. A. Berends, W. T. Giele and H. Kuijff, *Exact Expressions for Processes Involving a Vector Boson and Up to Five Partons*, *Nucl. Phys.* **B321** (1989) 39.
27. F. A. Berends and W. T. Giele, *Multiple Soft Gluon Radiation in Parton Processes*, *Nucl. Phys.* **B313** (1989) 595.
28. F. A. Berends, W. T. Giele and H. Kuijff, *Exact and Approximate Expressions for Multi - Gluon Scattering*, *Nucl. Phys.* **B333** (1990) 120.
29. S. Dittmaier, *Full $O(\alpha)$ radiative corrections to high-energy Compton scattering*, *Nucl. Phys.* **B423** (1994) 384 [hep-ph/9311363].
30. S. Dittmaier, *Weyl-van der Waerden formalism for helicity amplitudes of massive particles*, *Phys. Rev.* **D59** (1998) 016007 [hep-ph/9805445].
31. S. Weinzierl, *Automated computation of spin- and colour-correlated Born matrix elements*, *Eur. Phys. J.* **C45** (2006) 745 [hep-ph/0510157].
32. M. L. Mangano and S. J. Parke, *Multiparton amplitudes in gauge theories*, *Phys. Rept.* **200** (1991) 301 [hep-th/0509223].
33. L. J. Dixon, *Calculating scattering amplitudes efficiently, in QCD and beyond. Proceedings, Theoretical Advanced Study Institute in Elementary Particle Physics, TASI-95, Boulder, USA, June 4-30, 1995*, pp. 539–584, 1996, hep-ph/9601359.
34. H. K. Dreiner, H. E. Haber and S. P. Martin, *Two-component spinor techniques and Feynman rules for quantum field theory and supersymmetry*, *Phys. Rept.* **494** (2010) 1 [0812.1594].
35. H. Elvang and Y.-t. Huang, *Scattering Amplitudes*, **1308.1697**.
36. L. J. Dixon, *A brief introduction to modern amplitude methods*, in *Proceedings, 2012 European School of High-Energy Physics (ESHEP 2012): La Pommeraye, Anjou, France, June 06-19, 2012*, pp. 31–67, 2014, 1310.5353, DOI.
37. J. Alneftjord, A. Lifson, C. Reuschle and M. Sjö Dahl, *The chirality-flow formalism for the standard model*, *Eur. Phys. J. C* **81** (2021) 371 [2011.10075].
38. A. Lifson, C. Reuschle and M. Sjö Dahl, *Introducing the Chirality-flow Formalism*, *Acta Phys. Polon. B* **51** (2020) 1547.

39. A. Lifson, C. Reuschle and M. Sjö Dahl, *The chirality-flow formalism*, *Eur. Phys. J. C* **80** (2020) 1006 [2003.05877].
40. J. Alnefjord, A. Lifson, C. Reuschle and M. Sjö Dahl, *A Brief Look at the Chirality-Flow Formalism for Standard Model Amplitudes*, *PoS LHCP2021* (2021) 160 [2110.04125].
41. C. Degrande, C. Duhr, B. Fuks, D. Grellscheid, O. Mattelaer and T. Reiter, *UFO - The Universal FeynRules Output*, *Comput. Phys. Commun.* **183** (2012) 1201 [1108.2040].
42. P. de Aquino, W. Link, F. Maltoni, O. Mattelaer and T. Stelzer, *ALOHA: Automatic libraries of helicity amplitudes for Feynman diagram computations*, *Computer Physics Communications* **183** (2012) 2254–2263.
43. O. Mattelaer and K. Ostrolenk, *Speeding up MadGraph5_aMC@NLO*, *Eur. Phys. J. C* **81** (2021) 435 [2102.00773].
44. R. Kleiss, W. J. Stirling and S. D. Ellis, *A New Monte Carlo Treatment of Multiparticle Phase Space at High-energies*, *Comput. Phys. Commun.* **40** (1986) 359.
45. N. Nethercote and J. Seward, *Valgrind: a framework for heavyweight dynamic binary instrumentation*, in *PLDI '07*, 2007.
46. J. Weidendorfer, M. Kowarschik and C. Trinitis, *A tool suite for simulation based analysis of memory access behavior*, vol. 3038, pp. 440–447, 06, 2004, DOI.